Cancer Cell
Article

An Integrated In Vitro and In Vivo High-Throughput Screen Identifies Treatment Leads for Ependymoma

Jennifer M. Atkinson,[1] Anang A. Shelat,[2] Angel Montero Carcaboso,[3] Tanya A. Kranenburg,[1] Leggy A. Arnold,[2] Nidal Boulos,[1] Karen Wright,[1,4] Robert A. Johnson,[1] Helen Poppleton,[1] Kumarasamypet M. Mohankumar,[1] Clementine Féau,[2] Timothy Phoenix,[1] Paul Gibson,[1] Liqin Zhu,[1] Yiai Tong,[1] Chris Eden,[1] David W. Ellison,[5] Waldemar Priebe,[6] Dimpy Koul,[7] W. K. Alfred Yung,[7] Amar Gajjar,[4] Clinton F. Stewart,[3] R. Kiplin Guy,[2,*] and Richard J. Gilbertson[1,4,*]

[1]Department of Developmental Neurobiology
[2]Department of Chemical Biology and Therapeutics
[3]Department of Pharmacology
[4]Department of Oncology
[5]Department of Pathology
St. Jude Children's Research Hospital, 262 Danny Thomas Place, Memphis, TN 38105, USA
[6]Department of Experimental Therapeutics
[7]Department of Neuro-Oncology, Division of Cancer Medicine
University of Texas MD Anderson Cancer Center, Houston, TX 77030, USA
*Correspondence: kip.guy@stjude.org (R.K.G.), richard.gilbertson@stjude.org (R.J.G.)
DOI 10.1016/j.ccr.2011.08.013

SUMMARY

Using a mouse model of ependymoma—a chemoresistant brain tumor—we combined multicell high-throughput screening (HTS), kinome-wide binding assays, and in vivo efficacy studies, to identify potential treatments with predicted toxicity against neural stem cells (NSC). We identified kinases within the insulin signaling pathway and centrosome cycle as regulators of ependymoma cell proliferation, and their corresponding inhibitors as potential therapies. FDA approved drugs not currently used to treat ependymoma were also identified that posses selective toxicity against ependymoma cells relative to normal NSCs both in vitro and in vivo, e.g., 5-fluorouracil. Our comprehensive approach advances understanding of the biology and treatment of ependymoma including the discovery of several treatment leads for immediate clinical translation.

INTRODUCTION

Advances in cancer therapy have been made by testing empiric combinations of treatments in patients with histologically similar tumors. This clinical research has been supplemented by laboratory studies of human cancer cell lines and xenografts aimed at identifying therapies. Although this approach has reduced deaths from some common malignancies (Berry et al., 2005; Pui et al., 2004), it is inherently inefficient, failing to account for the different molecular subtypes that populate cancers, and providing little insight into the patients most likely to benefit from each therapy. This process is especially inadequate for developing treatments of rare cancers that have few patient numbers and limited preclinical tools.

Ependymomas are rare tumors of the brain and spinal cord that are incurable in up to 40% of cases (McGuire et al., 2009; Merchant et al., 2009). Treatment of this disease has changed little over the last 40 years and is essentially limited to surgery and radiation. Chemotherapy has not impacted survival from ependymoma, but the rarity of the disease and lack of preclinical

Significance

Trial therapies for rare cancers are usually selected empirically and often fail. The poor efficiency of this process is limited further by a lack of accurate preclinical models, and small patient numbers that may include distinct subtypes. More rational, evidence-based approaches to select and prioritize trial treatments are needed. Using HTS, kinome-wide binding assays, and in vivo efficacy studies, we interrogated an accurate mouse model of a specific subtype of human ependymoma. This comprehensive approach identified kinases not known to maintain ependymoma and several treatment leads with predicted NSC toxicity for immediate clinical translation. This approach holds significant promise to prioritize therapies for clinical trials among patients with specific subtypes of cancer.

models has precluded comprehensive drug testing (Bouffet and Foreman, 1999; Gilbert et al., 2010).

Histologic similarities between ependymomas from the different regions of the central nervous system (CNS) have led investigators to treat these tumors as a single entity. But these tumors include discrete subtypes that will likely require different therapies (Johnson et al., 2010; Taylor et al., 2005). To develop more rational treatments of ependymoma, we are generating mouse models of each disease subtype (Johnson et al., 2010). The first of these, mEP^{Ephb2}, faithfully recapitulates the histology and transcriptome of one form of human cerebral ependymoma (subtype-D), making it an attractive tool for developing treatments for this specific group of patients.

Recent evidence suggests that some cancers, including ependymomas, contain stem-like cancer cells that are both sufficient and required to propagate the disease (Johnson et al., 2010; Lapidot et al., 1994; Singh et al., 2004; Taylor et al., 2005). Therefore, the most effective treatments of these cancers are likely to include drugs that kill these cells (Zhou et al., 2009). However, ependymoma stem-like cells are remarkably similar to the normal NSCs from which they arise (Johnson et al., 2010), suggesting such treatments may also be toxic to developing tissues. Developmental toxicities are a particular concern when treating children with cancer whose organ systems are immature (Kimura et al., 2008). Our ependymoma model system generates tumors from isolated NSCs, allowing the conduct of comparative drug toxicity studies. The goal of the current study was to employ this mouse model system in a multiplatform, in vitro and in vivo drug development approach to identify subtype-specific therapies with predicted stem cell toxicity.

RESULTS

High-Throughput Screen (HTS) for Predicting Efficacy and Toxicity

Cells isolated from mEP^{Ephb2} ependymomas as well as distinct variants of mouse NSCs, maintain their functional and molecular identity when passaged clonally under conditions that promote stem cell growth (Johnson et al., 2010). As a first step to identify treatments of ependymoma, we adapted these cultures to perform in a HTS campaign that detected compound toxicity against normal and malignant stem cells with high reproducibility and sensitivity (Figure 1; Figure S1; Supplemental Experimental Procedures available online).

We screened a total of 7890 (5303 unique) compounds obtained from seven separate sources, divided among four libraries (Figure 1A): a "bioactive" library that included 5600 (3161 unique) bioactive compounds, natural products, and known drugs; a "kinase-scaffold" library composed of 1648 compounds designed using kinase inhibitor pharmacophore models; GlaxoSmithKline's Published Kinase Inhibitor Set (GSK-PKIS) composed of 367 kinase inhibitor tool compounds with good bioavailability and known specificity; and a Food and Drug Administration (FDA) library that included 275 FDA approved compounds that were enriched for anticancer and neurologically active drugs.

We first screened all compounds in the bioactive library, each at 8 μM concentration. This primary screen was conducted against mEP^{Ephb2} cells, as well as wild-type (NSC^{wt}), and *Ink4a/Arf*$^{-/-}$ (NSC^{null}) mouse embryonic forebrain NSCs—the initiating cell of mEP^{EphB2} tumors (Johnson et al., 2010). To increase the probability of identifying ependymoma-specific therapies, we also screened a nonependymoma mouse brain tumor that we generated by transducing NSC^{null} with the intracellular domain of NOTCH1 (mBT^{NICD1}; Figure S1). The scatterplot of control and test compound activity in this primary screen demonstrated a good separation between signal and noise for each cell type (Figure 1B). Potency was then assessed in a concentration response secondary screen for all compounds in the bioactive library that demonstrated ≥75% activity against any of the four cell types. This secondary screen was performed in triplicate using all four cell types. To assess the fidelity of the primary screen, we also included in the secondary screen an additional 254 compounds that demonstrated a range of primary screen activities <75%. Receiver operator characteristic (ROC) analysis of these data demonstrated good discriminatory power for each cell type, and indicated that a primary screen threshold of ≥50% activity would detect most true positives (Figure 1C). Having validated our primary and secondary screen using the bioactive library, we completed HTS of the kinase-scaffold, GSK-PKIS, and FDA libraries.

A total of 634 unique compounds across the four libraries, representing diverse drug classes, progressed from primary to secondary screening (Figure 1D). In all, 2.6% (n = 140/5303) of compounds displayed anti-mEP^{Ephb2} secondary screen activity (Figure 2). Since our HTS strategy included nonependymoma tumor cells and NSCs, we were able to refine our classification of compound activity (Table S1). To this end, we determined for each cell type, the average "effective concentration" of each compound that inhibited cell growth by 50% relative to control treatment (EC_{50}). The data were then used to identify compounds with ≥2-fold potency against mEP^{Ephb2} than other cells (0.08%, n = 4/5303; mEP^{Ephb2} selective); equally potent against mEP^{Ephb2} and mBT^{NICD1} cells relative to NSCs (0.04%, n = 2/5303; tumor selective); equally potent against all four cell types (2.5%, n = 134/5303; equipotent); ≥2-fold more potent against mBT^{NICD1} relative to all other cells (0.2%, n = 13/5303; mBT^{NICD1} selective); ≥2-fold more potent against NSCs (NSC^{wt} and/or NSC^{null}) relative to tumor cells (0.8%, n = 42/5303; NSC selective); inactive against mEP^{Ephb2} cells relative to all other cells (0.1%, n = 7/5303; mEP^{Ephb2} inactive); and inactive against all four cell types (91%, n = 4809/5303; inactive).

HTS Identifies Cell-Selective Activity that Varies with Drug Mechanism of Action

As expected, compounds with activity against mEP^{Ephb2} cells (mEP^{Ephb2} selective, tumor selective, and equipotent) were significantly enriched for anti-cancer drugs (Fisher's exact $p = 1.9 \times 10^{-7}$: Bonferroni correction threshold, p = 0.0016), but they displayed patterns of cell-selective activity that varied according to their mechanism of action (Figures 2 and 3). Almost all topoisomerase II inhibitors ($p = 7.6 \times 10^{-09}$) and microtubule poisons ($p = 4.0 \times 10^{-07}$) were equipotent against the four cell types. In contrast, dichotomous activity was observed among antimetabolite anticancer compounds. Antimetabolites that incorporate into DNA and disrupt normal DNA synthesis or methylation, e.g., decitabine, were all NSC selective ($p = 5.0 \times 10^{-09}$), while inhibitors of thymidylate synthase (TYMS) and/or

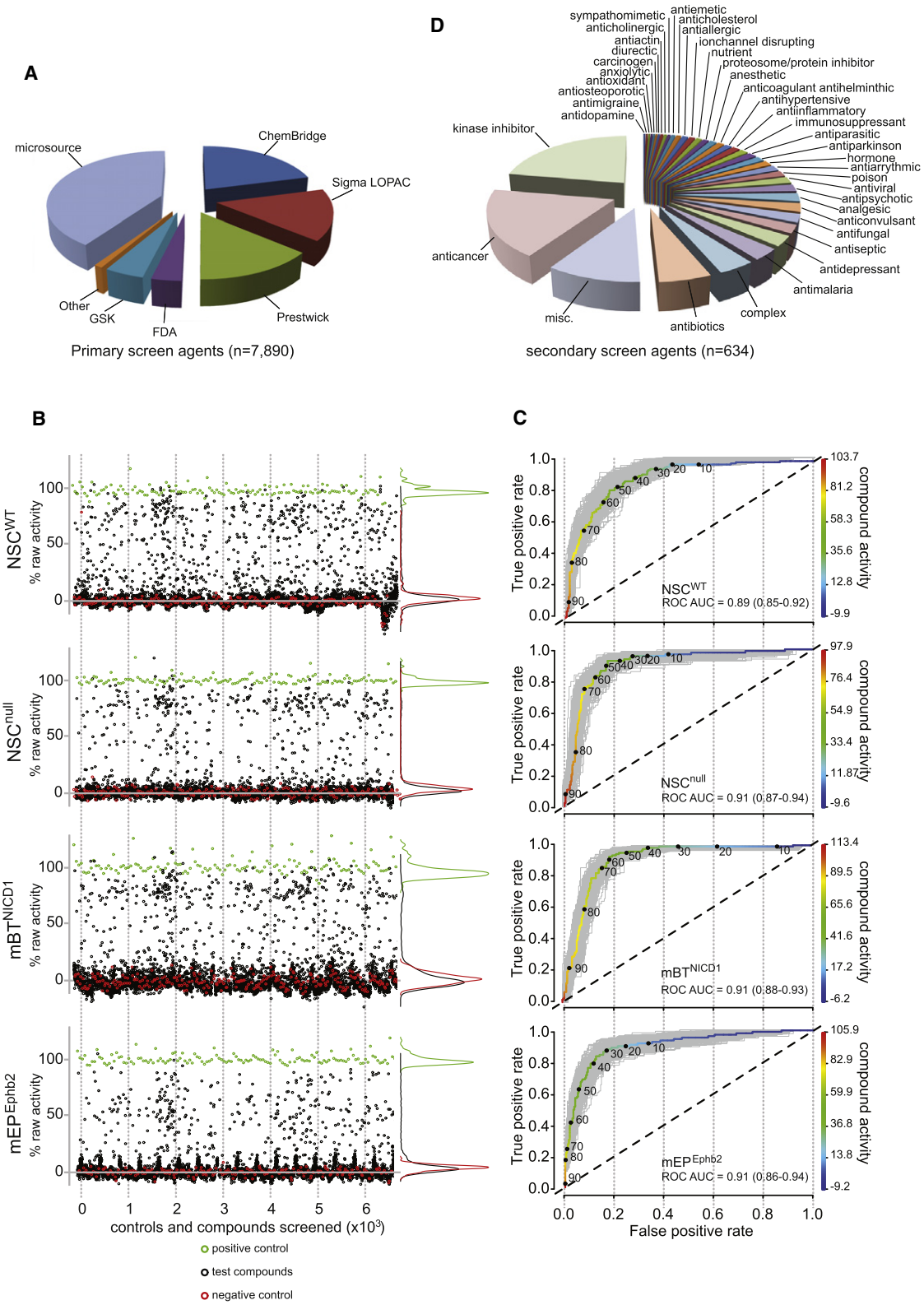

Figure 1. Compounds and Quality Control of the High-Throughput Screen

(A) Sources of compounds used in the screen.

(B) Scatter plot of percent primary screen activity (relative to vehicle) of positive controls (green) negative controls (red) and test compounds (black) for all four cell types.

dihydrofolate reductase (DHFR), e.g., 5-fluorouracil (5-FU), were enriched for ependymoma-selective compounds ($p = 5.0 \times 10^{-09}$). Indeed, three of the four ependymoma-selective compounds detected in the entire HTS were in this class: 5-FU, the 5-FU precursor 5-fluoro-5′-deoxyuridine, and the 5-FU derivative carmofur.

The fourth ependymoma-selective agent identified in our HTS—the ionophore beta-escin—disrupts normal membrane ion exchange. Interestingly, potassium ionophores were recently identified as breast cancer stem cell selective inhibitors, suggesting this drug class might have broad activity against malignant stem cell populations (Gupta et al., 2009). Proteosome or protein synthesis inhibitors included drugs that were NSC selective, e.g., bortezomib, while anticholesterol drugs were equipotent or tumor selective (Figures 2 and 3).

Integration of HTS and Kinome-Wide Binding Assays Unmasks Pathways Important for Maintaining Ependymoma Cells and NSCs

Active compounds detected by HTS were also enriched for inhibitors of specific kinases (Figures 2 and 3), including inhibitors of: Epidermal Growth Factor Receptor (EGFR, n = 9/11 inhibitors screened; $p = 1.0 \times 10^{-08}$); Insulin Growth Factor 1 Receptor (IGF1R, n = 5/5; $p = 7.3 \times 10^{-07}$); Polo-like kinase 1 (PLK1, n = 5/5; $p = 7.3 \times 10^{-07}$); Cyclin dependent kinase 2 (CDK2, n = 4/4; $p = 1.0 \times 10^{-05}$); and Jun NH(2)-terminal kinase 2 and 3(JNK2/3, n = 3/3; p = 0.0001). A single Glycogen Synthase Kinase 3β (GSK3β) inhibitor also proved active in secondary screening. The equipotent activity of EGFR inhibitors is compatible with reports that these receptors conduct critical signals in ependymoma and normal NSCs (Aguirre et al., 2010; Geoerger et al., 2008; Gilbertson et al., 2002; Mendrzyk et al., 2006); however, none of the other active kinase inhibitors identified, or their target molecules, have been suggested previously as treatments or drivers of ependymoma, respectively.

The finding that IGF1R and PLK1 inhibitors disrupt mEp^{Ephb2} cell and NSC proliferation is especially noteworthy. IGF1R is expressed at the apical surface of forebrain NSCs—the cell of origin of cerebral ependymoma (Johnson et al., 2010)—and activates NSC proliferation following binding of its ligand IGF2 that is contained within the cerebrospinal fluid (CSF) (Lehtinen et al., 2011). Furthermore, elevated levels of IGF2 sufficient to activate aberrant NSC proliferation are found in the CSF of patients with brain tumors (Lehtinen et al., 2011). The proliferation of NSCs and ependymoma stem cells occurs via a process termed asymmetric division by which the parent stem cell self-renews: this process is critically dependent on cell polarity, cell cycle timing, and mitotic spindle formation that are each regulated by PLK1 (Johnson et al., 2010; Noatynska et al., 2010; Wang et al., 2009). Thus, IGF1R and PLK1 inhibitors, of which more than 18 are currently in Phase I or II clinical trial, are attractive candidates for ependymoma clinical trials (Lens et al., 2010; Neal and Sequist, 2010). Importantly, several other kinase inhibitors currently under clinical development were inactive against mEP^{Ephb2}, e.g., BRAF inhibitors and BCR-ABL inhibitors, suggesting these drugs should given a lower priority for clinical trial in ependymoma.

In addition to inhibitors of known kinases, we also identified 13 equipotent orphan-kinase inhibitor scaffolds for which the molecular target is not known (Figures 2 and 3). Identifying the kinases targeted by these compounds could pinpoint further cell signals critical for ependymoma cell survival, as well as therapeutic approaches. Therefore, we subjected the four most active kinase scaffolds (SJ000516613, SJ000517447, SJ000517729, and SJ000517939; Figure 3) to competitive binding assays against 442 human kinases (see Supplemental Experimental Procedures). Kinase scaffolds were first screened at a single fixed concentration (2.5 μM) against all 442 kinases (Figure 4A). One or more kinase scaffolds bound 13 kinases with >50% activity relative to controls. In keeping with our HTS data, these included EGFR, Insulin Receptor-Related Receptor (INSRR), and EPHB2: the latter transforms NSCs in the mEP^{Ephb2} model. To validate additional kinases as potential drivers and drug targets of cerebral ependymoma, we performed a series of six-point dose response binding assays against kinases most tightly bound in the single concentration assay. These data identified PIP5K1C, TTK, and YSK4 as kinase targets of SJ000516613 and SJ000517729, with binding Kds similar to their EC_{50}s in whole-cell proliferation assays (Figures 3 and 4B). RIOK2 and CK1δ were bound by SJ000517939 and SJ000517447, respectively, albeit at much higher concentrations.

Integration of our HTS and kinome binding data showed that 57% (n = 25/44) of kinase inhibitors and scaffolds with activity against ependymoma cells and NSCs, target critical components of just three major cell pathways: the EGF, IGF and centrosome cycle pathways (Figures 3–5). Nine inhibitors targeted components of the centrosome cycle (Figure 5A), including PLK1 (discussed above), and CDK2 and its direct substrate TTK, that together regulate centrosome duplication (Cowan and Hyman, 2006; Kasbek et al., 2007). Seven inhibitors target the IGF pathway; including five direct inhibitors of IGF1R (Figure 5B and discussed above). Notably, gene expression profile analysis showed that IGF1R expression is significantly upregulated in mEP^{Ephb2} cells relative to parental NSCs or mBT^{NICD1} cells (Figure 5C). Further, GSK2110236A, a potent inhibitor of mEP^{Ephb2} proliferation (Figure 3) and known IGF1R kinase inhibitor within the GSK-PKIS library, blocked IGF1R and its downstream signal in mEP^{Ephb2} cells stimulated with IGF2 (Figure 5D). Together, these data identify the EGF, IGF, and centrosome cycle pathways as key signals for maintaining cerebral ependymoma and their corresponding inhibitors as lead candidate targets of therapies. However, the equipotent activity of these compounds in HTS should alert investigators to the possibility of NSC-toxicities in clinical trials.

(C) ROC analyses showing the true (y axis) versus false (x axis) positive rates of percent drug activity correlating the primary and secondary screens. The ROC curves in gray are calculated from 200 bootstrap simulations. Percent activity is color-coded according to the right y axis.
(D) Drug classes represented by the 634 compounds tested in secondary screens.
See also Figure S1.

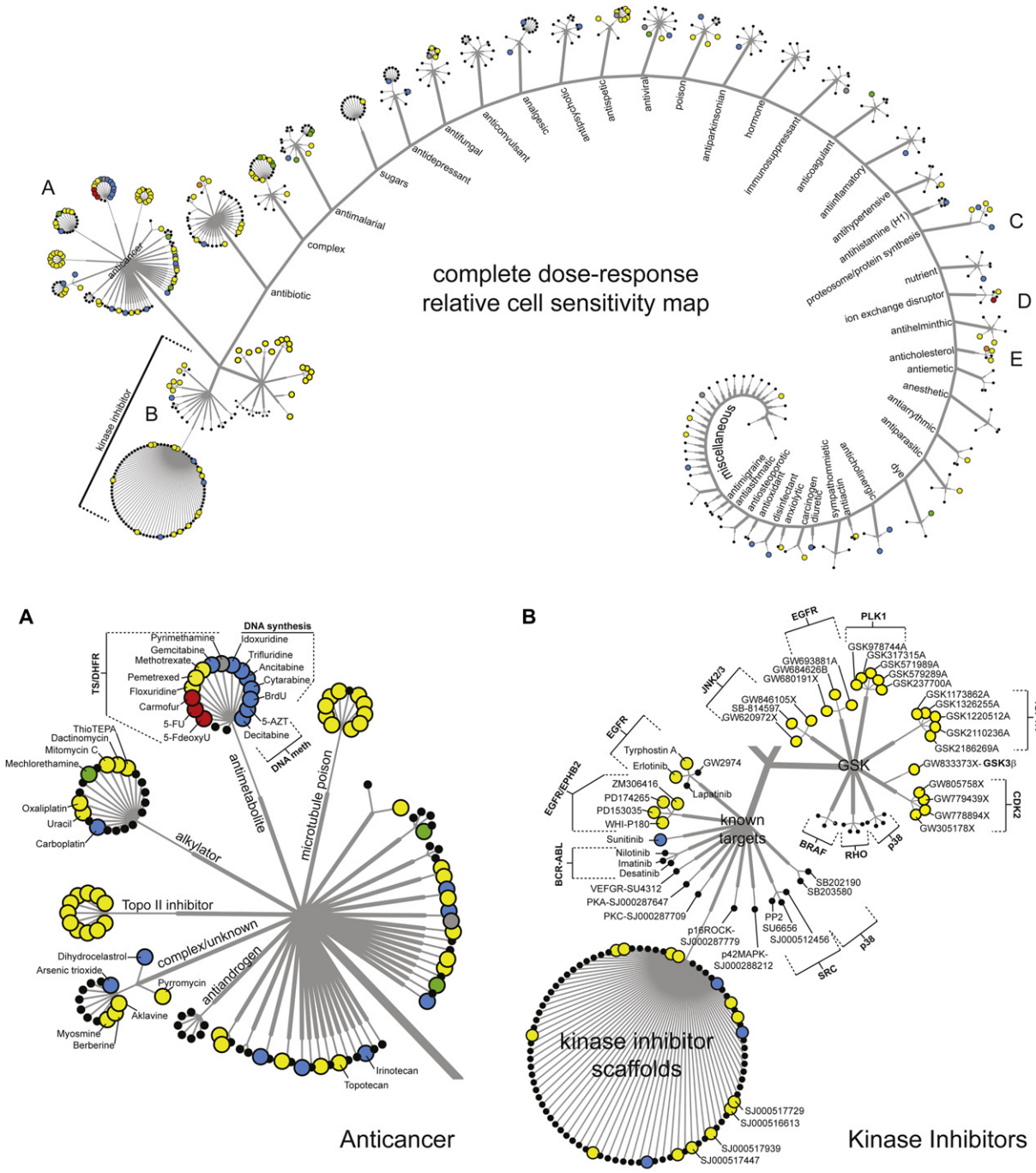
complete dose-response
relative cell sensitivity map
A
B
C
D
E
antibiotic
complex
antimalarial
sugars
antifungal
antidepressant
anticonvulsant
analgesic
antipsychotic
antiseptic
antiviral
poison
antiparkinsonian
hormone
immunosuppressant
anticoagulant
antiinflammatory
antihypertensive
antihistamine (H1)
proteosome/protein synthesis
nutrient
ion exchange disruptor
antihelminthic
anticholesterol
antiemetic
anesthetic
antiarrythmic
antiparasitic
dye
anticholinergic
sympathomimetic
vitamin
diuretic
carcinogen
anxiolytic
disinfectant
antioxidant
antiallergenic
antiasthmatic
antiestrogenic
antiprogestin
miscellaneous
kinase inhibitor
DNA synthesis
TS/DHFR
Pyrimethamine
Gemcitabine
Methotrexate
Pemetrexed
Floxuridine
Carmofur
5-FU
5-FdeoxyU
Idoxuridine
Trifluridine
Ancitabine
Cytarabine
BrdU
5-AZT
Decitabine
DNA meth
antimetabolite
microtubule poison
ThioTEPA
Dactinomycin
Mitomycin C
Mechlorethamine
Oxaliplatin
Uracil
Carboplatin
alkylator
Topo II inhibitor
Irinotecan
Topotecan
complex/unknown
Dihydrocelastrol
Arsenic trioxide
antiandrogen
Pyrvinium
Aklavine
Myosmine
Berberine
Anticancer
EGFR
PLK1
JNK2/3
GSK978744A
GSK317315A
GW693881A
GSK571989A
GW684626B
GSK579289A
GW680191X
GSK237700A
GW846105X
SB-814597
GW620972X
GSK1173862A
GSK1326255A
GSK1220512A
GSK2110236A
GSK2186269A
IGF1R
GSK
GW833373X- GSK3β
GW805758X
GW779439X
GW778894X
GW305178X
CDK2
EGFR
Tyrphostin A
Erlotinib
GW2974
Lapatinib
EGFR/EPHB2
ZM306416
PD174265
PD153035
WHI-P180
Sunitinib
known targets
BRAF
RHO
p38
BCR-ABL
Nilotinib
Imatinib
Desatinib
VEFGR-SU4312
PKA-SJ000287647
PKC-SJ000287709
SB202190
SB203580
PP2
SU6656
SJ000512456
p16ROCK-SJ000287779
p42MAPK-SJ000288212
p38
SRC
kinase inhibitor scaffolds
SJ000517729
SJ000516613
SJ000517939
SJ000517447
Kinase Inhibitors
C
Beta-dihydrorotenone
Cyclohexamide
Dihydrorotenone
Rotenone
Isorotenone
Bortezomib
proteosome
protein synthesis
D
Calmidazolium
Beta-Escin
ion exchange
disruptor
E
Simvastatin
Atorvastatin
Compactin
anticholesterol
activity class
relative ependymoma activity
mEP EPHB2 selective
tumor selective
equipotent
ependymoma 'active'
mBT NICD1 selective
NSC selective
mEP Ephb2 inactive
inactive
ependymoma 'inactive'

5-FU and Bortezomib Are Active against mEP^{Ephb2} Ependymoma In Vivo

To allow the most rapid translation of treatments from our HTS to the clinic, we selected two FDA approved anticancer drugs for our first sets of in vivo studies. 5-FU is a well-established chemotherapeutic for the treatment of certain cancers, e.g., colorectal cancer (Douillard et al., 2000; IMPACT, 1995), but this drug has not been tested formally in patients with ependymoma. The ependymoma-selective activity of 5-FU in our HTS and relatively low expression of TYMS (Figure 5C) —the principal cellular target of 5-FU—in mEP^{Ephb2} cells, suggest this drug as a rational treatment of cerebral ependymoma (Longley et al., 2003). Similarly, bortezomib—a reversible inhibitor of the 26S proteasome—has not been tested against ependymoma in the clinic but was highly potent against mEP^{Ephb2} cells, and has activity against a variety of cancers including brain tumors (Adams, 2004; Phuphanich et al., 2010; Richardson et al., 2003; Taniguchi et al., 2009).

First, we tested the in vivo efficacy of 5-FU and bortezomib using a robust orthotopic allograft model of mEP^{Ephb2} ependymoma. 1.5 × 10^6 mEP^{Ephb2} cells transduced with luciferin (hereon, mEP$^{Ephb2\text{-}LUC}$) were injected stereotactically into the brains of immunocompromised mice. Bioluminescence detected brain tumors in these mice that conferred a median survival of 31 days (n = 56 control mice) and displayed a histology and gene expression profile indistinguishable from that of mEP^{Ephb2} (Figure 6, Figure S2). Mice bearing mEP$^{Ephb2\text{-}LUC}$ tumors were treated with eight different therapeutic regimens (n ≥ 10 mice per cohort; Table 1). 5-FU and bortezomib were given intravenously at doses reported previously to be efficacious in cancer bearing mice (Houghton et al., 1996; Williamson et al., 2009). 5-FU is usually given as a prolonged infusion in the clinic; therefore, to simulate this, we also administered 5-FU via subcutaneous Alzet pumps (Kamano et al., 1997). For comparative purposes we also treated cohorts of mice with carboplatin, topotecan, irinotecan, or carboplatin plus topotecan that have produced clinical, but not durable, responses against ependymoma (Bomgaars et al., 2006; Bouffet and Foreman, 1999; Kadota et al., 1999). Neither carboplatin nor irinotecan were active against mEP^{Ephb2} in our HTS, while topotecan was moderately equipotent against all cells (EC_{50} = 0.2–0.7 μM; Figure 2). As an additional test of the power of our HTS to predict in vivo efficacy, we treated a cohort of mice with lapatinib that was inactive in our HTS, but is currently undergoing clinical trials in ependymoma. Each of these chemotherapies were administered according to existing preclinical regimens (Gorlick et al., 2009; Stewart et al., 2004; Thompson et al., 1997; Tonda et al., 1996; Wagner et al., 2010) or schedules designed to generate plasma levels in mice that are equivalent to those active in children with brain tumors (Table 1). Each protocol group was paired with a control group of five or more mice that were implanted with mEP$^{Ephb2\text{-}LUC}$ cells, treated with vehicle alone, and imaged in parallel at weekly intervals by bioluminescence (Figure 6).

In keeping with the relative resistance of ependymoma to chemotherapies and the results of our HTS, carboplatin, topotecan, irinotecan and lapatinib were all inactive against mEP$^{Ephb2\text{-}LUC}$ brain tumors (Figure 6). In stark contrast, both bortezomib and intravenous 5-FU halved the rate of mEP$^{Ephb2\text{-}LUC}$ tumor growth and significantly prolonged the survival of mice harboring these tumors. These data support our HTS as a relatively accurate tool for predicting in vivo drug efficacy. In contrast to intravenous 5-FU, this drug was inactive when delivered subcutaneously (Figure 6). To test if pharmacokinetic differences might account for the variation in efficacy between intravenous and subcutaneous administered 5-FU, we allowed mEP$^{Ephb2\text{-}LUC}$ tumors to form around microdialysis catheters in the brains of recipient mice and measured simultaneously the concentration of 5-FU in the plasma and tumor following intravenous or subcutaneous drug administration (Supplemental Experimental Procedures). Intravenous 5-FU produced a concentration in brain tumors that peaked at 800 μM ± 79 SD, and remained above 10 μM for approximately 1 hr: an exposure profile shown by in vitro wash-out experiments to kill 90% of mEP^{Ephb2} cells (Figures 7A and 7B). In contrast, subcutaneous infusions of 5-FU at our trial dose of 1.03 mg/kg/hr failed to generate detectable tumor drug levels (data not shown). Experiments using the maximum amount of 5-FU deliverable via Alzet pumps (13 mg/kg/hr) maintained 5-FU tumor concentrations of approximately 10 μM for over 24 hr, but this schedule was unacceptably toxic (≥20% weight loss) precluding assessment of in vivo therapeutic efficacy. Together these data identify bortezomib and 5-FU as potential treatments of ependymoma and indicate that the mode of administration of 5-FU should be given careful consideration when planning the treatment of ependymoma.

HTS Predicts Patterns of 5-FU and Bortezomib NSC Toxicity In Vivo

Our HTS was designed to predict the NSC toxicity of compounds as well as their efficacy against ependymoma. Since this information could prove extremely useful when prioritizing agents for clinical trials we sought to test in vivo the prediction from our HTS, that bortezomib would be relatively more toxic than 5-FU to NSCs (Figures 2 and 3).

Assessing the relative toxicity of drugs in vivo is complex because it is difficult to regulate drug levels in tissues, and tissue damage can involve multiple cell types. Nevertheless, we reasoned that the schedules of 5-FU and bortezomib that displayed equivalent efficacy against ependymomas in the brain (Figure 6, difference in median survival p = 0.1 and no significant difference in tumor growth at any time point) are clinically meaningful schedules for comparative studies of NSC toxicity. We treated nontumor-bearing mice with therapeutically equivalent schedules of 5-FU, bortezomib, or vehicle control, and after 2 or 4 weeks of therapy, measured the rate of apoptosis, and extent of doublecortin (DCX) positive neuroblast rests in the

Figure 2. Drug Class Network Tree of Cell Type-Specific Potencies of 634 Compounds Subjected to Secondary Screening

Top figure shows compounds clustered according to major therapeutic indication and mechanism of action. (A)–(E) indicate the location of larger figures shown below. Activity was determined by dose response in secondary screening. Drug labels are colored according to cell type activity as defined in the key (bottom right). See also Table S1.

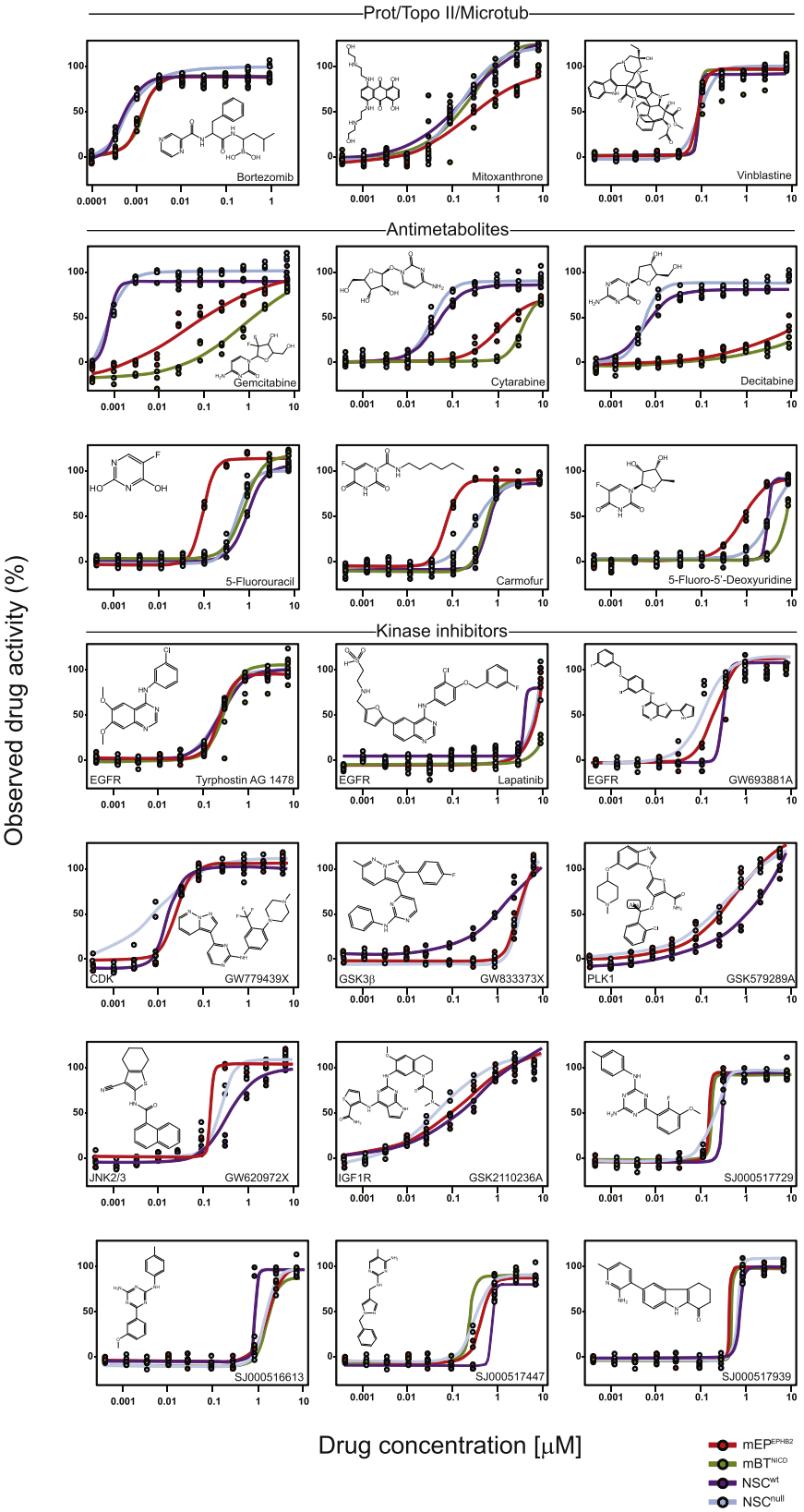

Figure 3. Patterns of Drug Class Sensitivity among Cells

Dose-response curves reveal distinct patterns of relative drug sensitivity among normal NSCs and tumor cells. The structure of the corresponding agent (and where appropriate molecular target) is shown in each graph.

subventricular zone (SVZ; Figure 7E). The accumulation of apoptotic neuroblasts is an established feature of ischemic, chemotherapeutic, and genetic damage to the SVZ (Baker et al., 2006; Brown et al., 2003; Carlén et al., 2009; Dietrich et al., 2006; Jin et al., 2010). To provide an additional measure of the cellular response to drugs we used $Prom1^{+/C\text{-}L}$ mice in our studies: these mice express the LacZ reporter from the Prom1 locus in NSCs, neuroblasts, and ependymal cells (Coskun et al., 2008; Kriegstein and Alvarez-Buylla, 2009; Zhu et al., 2009).

Following 2 weeks of therapy, the number of apoptotic cells in the SVZ of 5-FU and bortezomib-treated mice was double (12.0 ± 1.7 SEM, $p < 0.05$) and more than triple (22.2 ± 5.1 SEM, $p < 0.005$) that of controls (6.3 ± 1.2 SEM), respectively (Figure 7E). Bortezomib also quadrupled the area of DCX^+ neuroblast rests in the SVZ (6.0 μm^2 ± 0.6 per μm ventricular surface versus control = 1.5 μm^2 ± 0.6 per μm ventricular surface; $p < 0.005$); but 5-FU therapy had no significant impact on DCX labeling (2.2 μm^2 ± 1.1 per μm ventricular surface). Both 5-FU (35.1% ± 3.3% SEM, $p < 0.05$) and bortezomib (39.2% ± 2.8% SEM, $p < 0.005$) increased the number of $Prom1^+$ cells in the SVZ at 2 weeks relative to controls (20.9 ± 2.4 SEM; Figure 7E). Following 4 weeks of therapy, apoptotic and DCX^+ labeling in the SVZ of both 5-FU and bortezomib-treated mice returned to control levels (Figure 7E); however, $Prom1^+$ cell numbers continued to rise in the SVZ of bortezomib-treated mice, reaching >2.5 times that of controls by 4 weeks (57.8% ± 4.0% SEM versus control = 19.4% ± 3.1% SEM, $p < 0.0005$; Figure 7E). These cells included a mix of $Prom1^+/CD24^+$ ependymal cells, as well as a large number of $Prom1^+/CD24^-$ cells that likely represent NSCs and neuroblasts (Figure 7F). These data strongly suggest that bortezomib is more damaging to the SVZ niche than therapeutically equivalent doses of 5-FU, and provide preliminary evidence that our HTS might be useful for predicting the NSC toxicity of potential ependymoma therapies. Further work is required to fully characterize the expanded $Prom1^+$ SVZ cell population in drug-treated mice, and to determine the clinical significance of histologic SVZ damage.

DISCUSSION

The approach described here should significantly advance the efficiency and speed with which we discover and develop treatments for rare cancers and cancer subtypes. Studies of genetic mouse models have uncovered treatments for some brain tumors (Romer et al., 2004; Rudin et al., 2009), but a lack of ependymoma models has precluded similar efforts for this disease. We describe an integrated, multiplatform, in vitro and in vivo drug screen of an accurate mouse model of ependymoma (mEP^{Ephb2}), identifying the IGF, EGF, and centrosome cycle pathways as key candidate regulators of subtype-D tumors, as well as several treatment leads for the disease. We believe that these treatments are significantly enriched for drugs that will ultimately prove effective in patients because mEP^{Ephb2} tumors reproduce the histology, ultrastructure, and transcriptome of subtype-D ependymoma with remarkable fidelity (Johnson et al., 2010).

Ependymomas retain many of the biological properties of their parent NSCs (Johnson et al., 2010). Therefore, many potent antiependymoma drugs may also be neurotoxic. This notion is supported by the results of our HTS, in which the majority of active agents, including molecular targeted therapies, were equipotent against ependymoma and NSCs. Although similarities between ependymoma and NSCs may mean that cancer-selective agents are rare, our HTS system can identify these drugs. This represents a significant advance for clinical trial design. For example, ependymoma-selective agents (e.g., 5-FU) may be paired with effective but less selective drugs, to maximize efficacy while minimizing overlapping toxicity. Preclinical optimization of appropriate drug combinations for clinical trial in rare cancers is especially important, since the small patient populations place severe constraints on the number of clinical studies that can be conducted.

It is important to note that mEP^{Ephb2} tumors model just one (subtype-D) of nine possible subtypes of human ependymoma (Johnson et al., 2010). Therefore, some drugs identified in the current study may retain subtype-D specificity in humans, rather than displaying broad antiependymoma activity; however, this is a strength rather than a weakness of our approach. Although many human cancers have been carved up into distinct subtypes, these are not usually considered in the clinical trial design because we have lacked the means to predict their sensitivity to drugs. Consequently, clinical trials that fail to recruit adequate numbers of treatment-sensitive patients run the risk of rejecting useful drugs. Accurate mouse models of genomic subtypes of cancers present the exciting opportunity to model human cancer heterogeneity during preclinical drug development. To this end, we are using the same methodology employed to produce mEP^{Ephb2} tumors to generate mouse models of the remaining eight ependymoma subtypes. Together with our integrated in vitro and in vivo screening approach, this battery of models should allow us to complete in months, numerous single and multidrug preclinical trials that would take decades to conduct in the clinic. Drugs prioritized through this approach could then be passed to definitive clinical trials.

The active agents identified in our study not only provide therapeutic leads for the clinic but also insights into disease biology. Specifically, our combined HTS and kinome-wide binding assays of active kinase inhibitor scaffolds, have unmasked the IGF signaling and centrosome cycle pathways as regulators of subtype-D ependymoma. Further work will be required to define the aberrant function and clinical significance of these pathways, but studies of normal NSCs strongly suggest that these pathways are likely to be important in ependymoma. Lehtinen and colleagues showed recently that the CSF provides a proliferative niche for forebrain NSCs that includes IGF2 as a major constituent. Specifically, they demonstrated that IGF2 present in the CSF is bound by IGF1R expressed in the apical membranes of NSCs, stimulating cell proliferation (Lehtinen et al., 2011). The vast majority of ependymomas arise directly adjacent to the ventricular system, most likely from NSCs of the SVZ (Johnson et al., 2010; Kleihues et al., 2002; Taylor et al., 2005). Furthermore, we show here that IGF1R is upregulated in mEP^{Ephb2} cells relative to their parental NSCs, and that IGF2-IGF1R signaling in these cells is blocked by drugs that inhibit their proliferation.

Considerable evidence also points to the centrosome cycle as a critical regulator of NSC polarity, self-renewal, and proliferation (Lesage et al., 2010). In this regard, Wang and colleagues

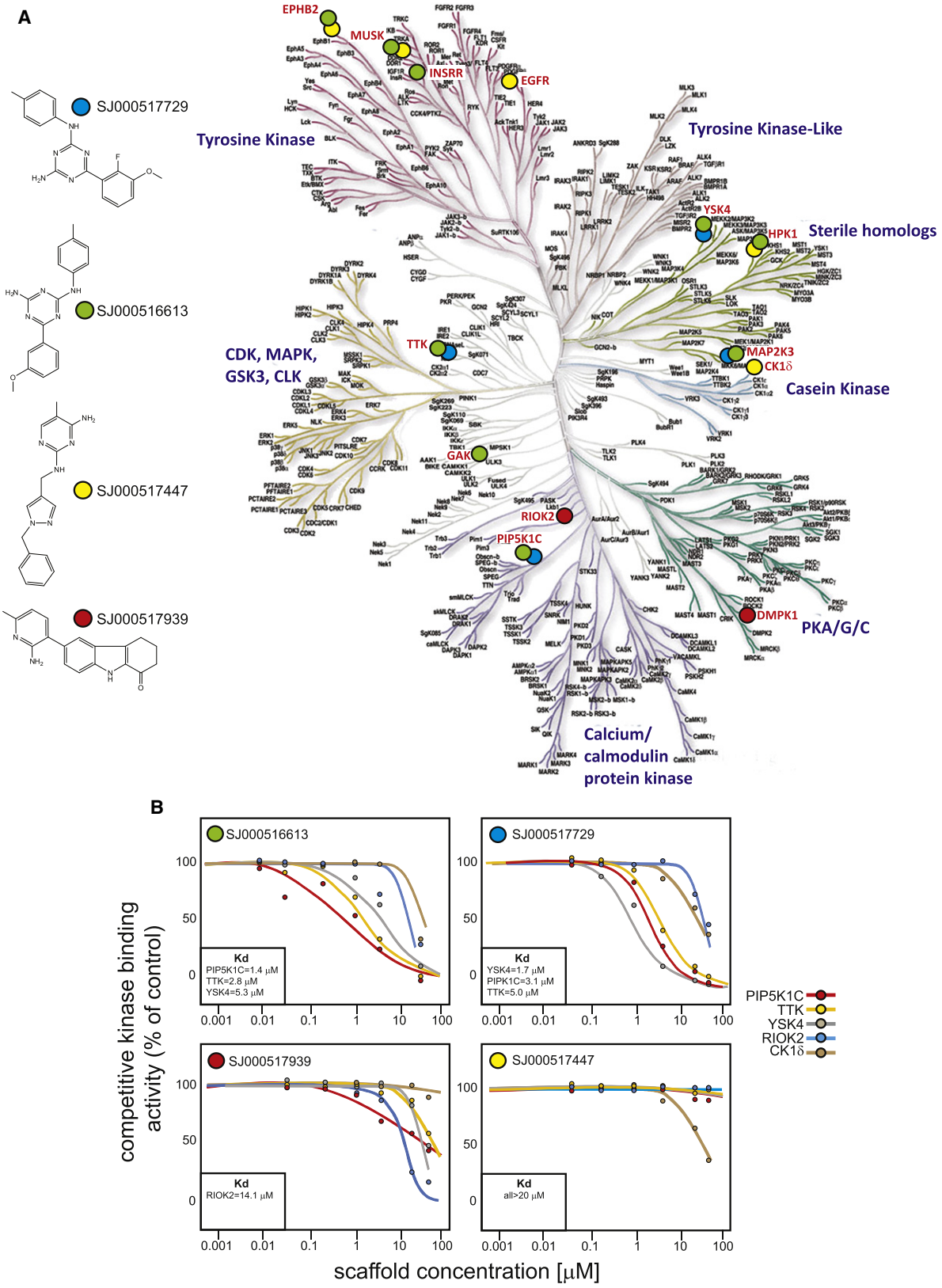
A
SJ000517729
SJ000516613
SJ000517447
SJ000517939
EPHB2
MUSK
INSRR
EGFR
YSK4
HPK1
TTK
MAP2K3
CK1δ
GAK
RIOK2
PIP5K1C
DMPK1
Tyrosine Kinase
Tyrosine Kinase-Like
Sterile homologs
CDK, MAPK, GSK3, CLK
Casein Kinase
PKA/G/C
Calcium/ calmodulin protein kinase
B
SJ000516613
SJ000517729
SJ000517939
SJ000517447
Kd
PIP5K1C=1.4 μM
TTK=2.8 μM
YSK4=5.3 μM
Kd
YSK4=1.7 μM
PIPK1C=3.1 μM
TTK=5.0 μM
Kd
RIOK2=14.1 μM
Kd
all>20 μM
PIP5K1C
TTK
YSK4
RIOK2
CK1δ
competitive kinase binding activity (% of control)
scaffold concentration [μM]

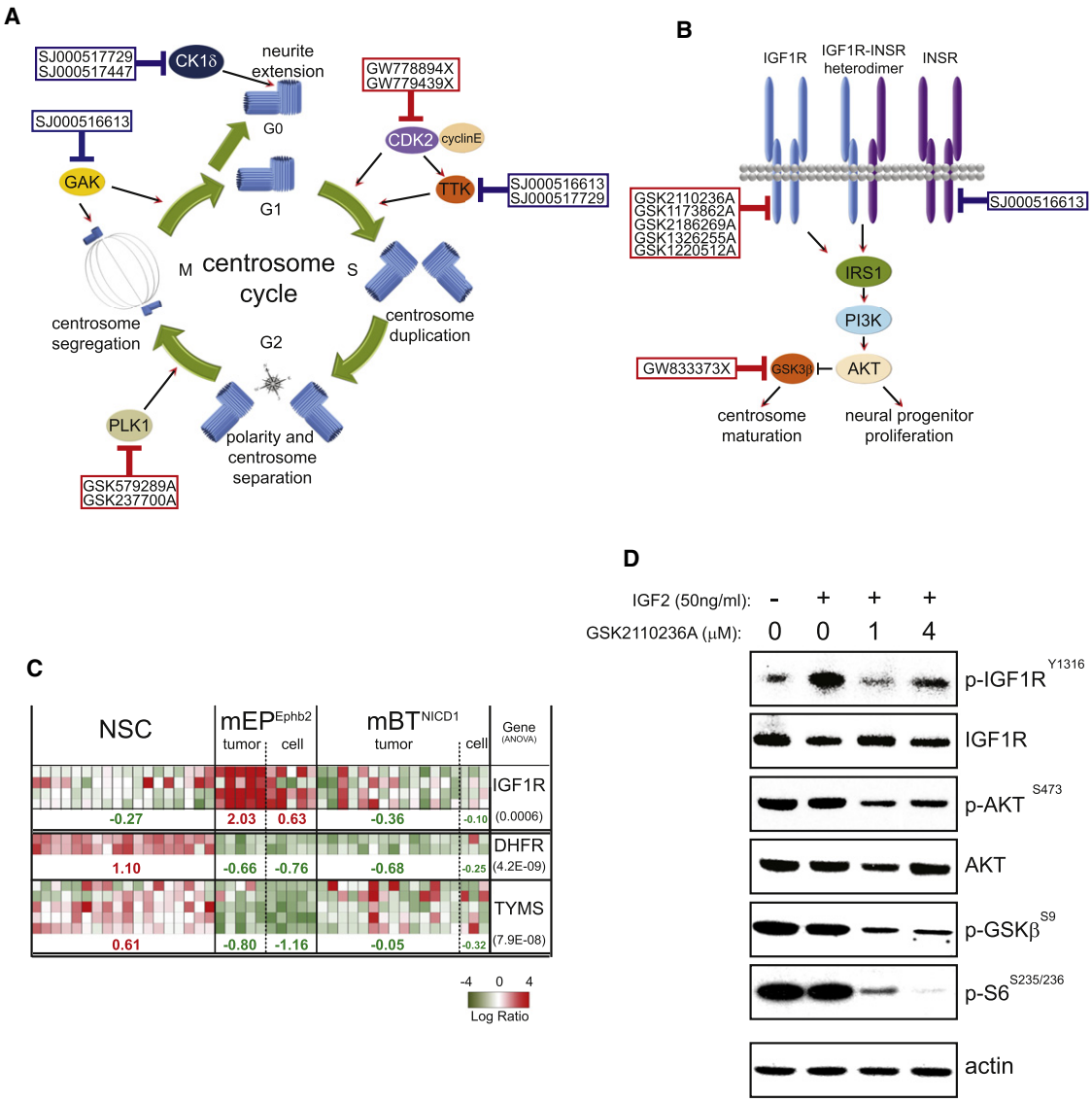

Figure 5. Kinase Inhibitors Active against mEP^{Ephb2} Target the Centrosome Cycle and Insulin Growth Factor Signaling Pathway

(A and B) Schematics of the centrosome cycle (**A**) and insulin growth factor pathway (**B**) marked with members of the kinase inhibitor scaffold (blue boxes) and GSK-PKIS (red boxes) libraries adjacent to their target molecules.

(C) Heatmaps reporting gene expression patterns in mouse cells and tumors (data from Johnson et al., 2010) of IGF1R, DHFR and TYMS. Figures below report the median Log Ratio of expression for each cell or tumor type and the number in parenthesis to the right the p-value for the ANOVA of this distribution.

(D) Western blot analysis of phosphorylated and total IGF1R, AKT, and phosphorylated GSK3β and S6 species in mEP^{Ephb2} cells treated with the IGF1R kinase inhibitor GSK2110236A (or vehicle) followed by IGF2 stimulation.

showed that the centrioles are preferentially inherited during the asymmetric division of mouse NSCs, such that the renewed daughter inherits the maternal centriole while the new centrosome is inherited by the differentiating daughter neuroblast (Wang et al., 2009). Many of the inhibitors the we identified as active against mEP^{Ephb2} cells and NSCs, target kinases that regulate critical steps in this process including centrosome duplication, e.g., CDK2 and TTK; spindle orientation and centrosome separation, e.g., PLK1; and spindle maintenance, e.g., GAK. Thus, the centrosome cycle is intimately related to NSC fate and may well be disrupted and targetable in ependymoma. We are currently working to determine the roles of PIP5K1C

Figure 4. Kinome-Wide Binding Assay of Equipotent Kinase Inhibitor Scaffolds

(A) Left, four kinase inhibitor scaffolds with equipotent activity in the HTS were subject to a single concentration (2.5 μM) competitive binding assay against 442 kinases in the human kinome (right). Kinases bound with more than 50% activity relative to controls are marked with labels colored according to scaffold. Reproduced courtesy of Cell Signaling Technology, Inc. (www.cellsignal.com).

(B) Six-point dose-response Kd binding assays of scaffolds against selected kinases. Boxes show the Kd values (≤20 μM) for each kinase.

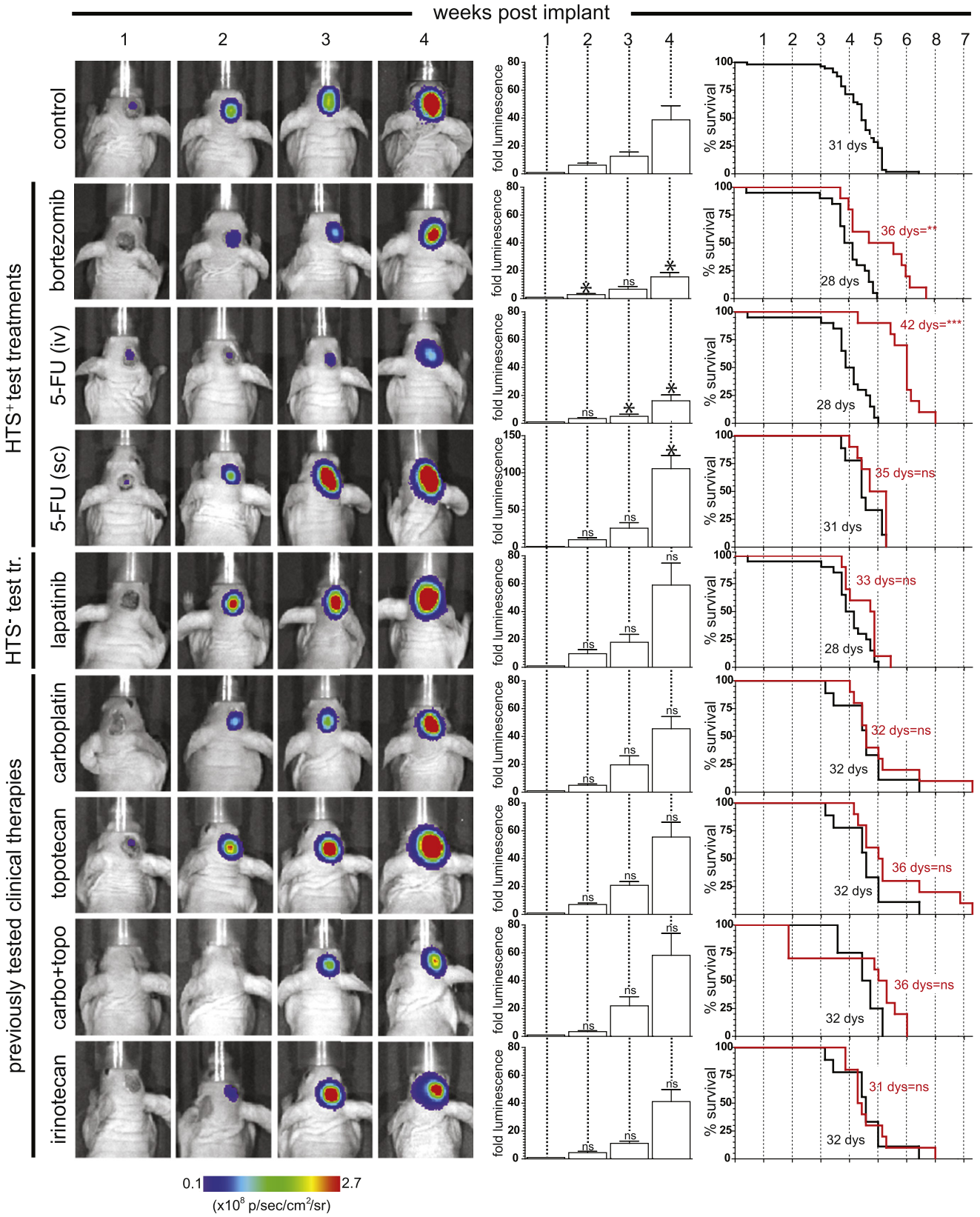
weeks post implant
1
2
3
4
control
bortezomib
5-FU (iv)
5-FU (sc)
lapatinib
carboplatin
topotecan
carbo+topo
irinotecan
HTS+ test treatments
HTS- test tr.
previously tested clinical therapies
fold luminescence
% survival
31 dys
36 dys=**
28 dys
42 dys=***
28 dys
35 dys=ns
31 dys
33 dys=ns
28 dys
32 dys=ns
32 dys
36 dys=ns
32 dys
36 dys=ns
32 dys
31 dys=ns
32 dys
ns
*
0.1
2.7
(x10^8 p/sec/cm^2/sr)

Table 1. Preclinical Drug Protocols Used to Treat Mice Harboring mEP^{Ephb2} Orthotpic Xenografts

Drug	Dose (per kg)	Schedule	Reference
5-FU	75 mg	i.v., once weekly	Houghton et al., 1996
5-FU	Up to 15 mg	s.c., implants	Kamano et al., 1997
Bortezomib	0.8 mg	i.v., twice weekly	Williamson, et al., 2009
Lapatinib	160 mg	p.o., twice daily 5/7 days	Gorlick et al., 2009
Irinotecan	10 mg	i.p., once daily × 5 days, recur every 21 days	Thompson et al., 1997
Topotecan	1 mg	i.p., once daily × 5 days, recur every 21 days	Stewart et al., 2004
Carboplatin	90 mg	i.v., once every 21 days	Tonda et al., 1996
Topotecan + carboplatin	As above	As above	As above

i.v., intravenous; s.c., subcutaneous; i.p., intraperitoneal.

and YSK4 kinases in NSCs and mEP^{Ephb2} cells that were also identified in our kinome-wide binding assays but are less well understood. Notably, PIP5K1C that bound three of four kinase scaffolds in our screen maps to a focal amplicon that we observed in human cerebral ependymomas (19p13.3) and has been reported to maintain stem cell proliferation and inhibit neuronal differentiation (Johnson et al., 2010; Wang et al., 2007; Yu et al., 2011). Thus, this kinase is of particular interest as a potential therapeutic target in ependymoma.

Our study also emphasizes the value of HTS for drug retooling. 5-FU is active against glioblastoma but this drug has never been tested formally in patients with ependymoma (Grunda et al., 2010). Indeed, in the absence of the evidence provided in the current study, it is unlikely that an early generation chemotherapeutic like 5-FU would ever be selected for clinical trial against ependymoma. Therefore, HTS approaches provide us with the opportunity to rationally repurpose cancer drugs. Well-characterized and accurate models should improve the efficiency and the confidence with which we do this. When these studies are coupled with comprehensive pharmacokinetic studies, these models can also help determine the most appropriate mode of administration of repurposed drugs. Concurrent measures of brain tumor and plasma 5-FU levels in our model suggest that bolus administration might be a more effective way to deliver the drug to ependymoma. Importantly, we are now using these preclinical response and pharmacokinetic models to test combinations of drugs identified as most active in our single agent HTS and in vivo studies. This includes combinations of centrosome cycle or IGF inhibitors, with conventional cytotoxic agents such as 5-FU. We envisage that continued pharmacokinetic and response assessments of these combination therapies will allow us to design the optimal schedule for translation to the clinic.

In summary, we describe an integrated, multiplatform in vitro and in vivo HTS of ependymoma that identifies a series of biological insights and potential therapies for clinical development. Our mouse model allows both testing of drug efficacy in a specific genomic subtype of the disease, and concurrent assessment of toxicity to the parental normal NSC. The development of additional mouse models of ependymoma subtypes should allow further comprehensive preclinical assessment of therapies for clinical trials tailored to all disease subtypes.

EXPERIMENTAL PROCEDURES

Isolation and Culture of Mouse NSCs and Mouse Ependymoma Cells

mEP^{Ephb2} cells, mBT^{NICD1} cells, and mouse embryonic cerebral NSC^{wt} and NSC^{null} were isolated and cultured in supplemented neurobasal medium exactly as described previously (Johnson et al., 2010). mEP^{Ephb2} cells were tagged with luciferase by transduction with an MSCV-Luc-IRES-YFP retrovirus. All animal studies, were approved by the St Jude Children's Research Hospital Animal Care and Usage Committee and performed in full compliance with regulatory standards.

HTS

The HTS approach is described in detail in Supplemental Experimental Procedures. Briefly, for primary screening cells were seeded in 30 μl of neurobasal medium in each well of 384-well plates (Corning) using an automated plate filler (Wellmate, Matrix). After 24 hr, 25 nl of solution containing appropriate compounds were pin transferred into the 384-well plates resulting in approximately 8.3 μM final drug concentration. Each plate also included DMSO only negative controls and cyclohexamide single point (0.5 μM) and dose-response (0.5 μM to 0.01 nM) positive controls. Cell number was determined in each well using the Cell Titer Glo reagent (Promega) and read in an automated Envision plate reader (Perkin-Elmer) after 96 hr incubation. Luminescence data were normalized by $\log_{10}$ transformation and the percentage inhibition = 100 × (sample result − negative control mean)/(positive control mean − negative control mean) calculated. Secondary screens were conducted in a similar manner although compounds were applied in a dilution series (8.3 μM to 0.5 nM final concentration) and repeated in triplicate. All data processing and visualization was performed using custom programs written in the Pipeline Pilot platform (Accelrys, v.7.0.1) and the R program. The R *drc* package was used to fit sigmoidal curves and ROC statistics computed using the R *rocr* package. The quality of the primary screening strategy was assessed by multiple methods including ROC analysis, Z-prime, and other screening quality metrics (see Supplemental Experimental Procedures).

Kinome-Wide Competitive Binding Assays

Kinome-wide binding assays were completed for kinase inhibitor scaffolds using KINOMEscan technology through DiscoveRx. Briefly, KINOMEscan is based on a competition binding assay that quantitatively measures the ability

Figure 6. In Vivo Efficacy against mEP^{Ephb2} Ependymomas of Drugs Displaying Different Activities in the HTS

Panels to the left show serial weekly bioluminescence scans of a single representative animal treated with the indicated drug(s). Central bar graphs report for the entire cohort of mice treated with the corresponding drug(s) the mean (±SD) weekly fold change in tumor bioluminescence relative to levels immediately following implantation. Asterisks in bar graphs of drug-treated mice report whether the fold tumor bioluminescence at that time point differs from that observed in the control group. Graphs to the right report the survival of drug- (red line) versus control- (black line) treated mice in each cohort. In both graphs *p = 0.05; **p = 0.005; ***p = 0.0005 for the corresponding statistic. See also Figure S2.

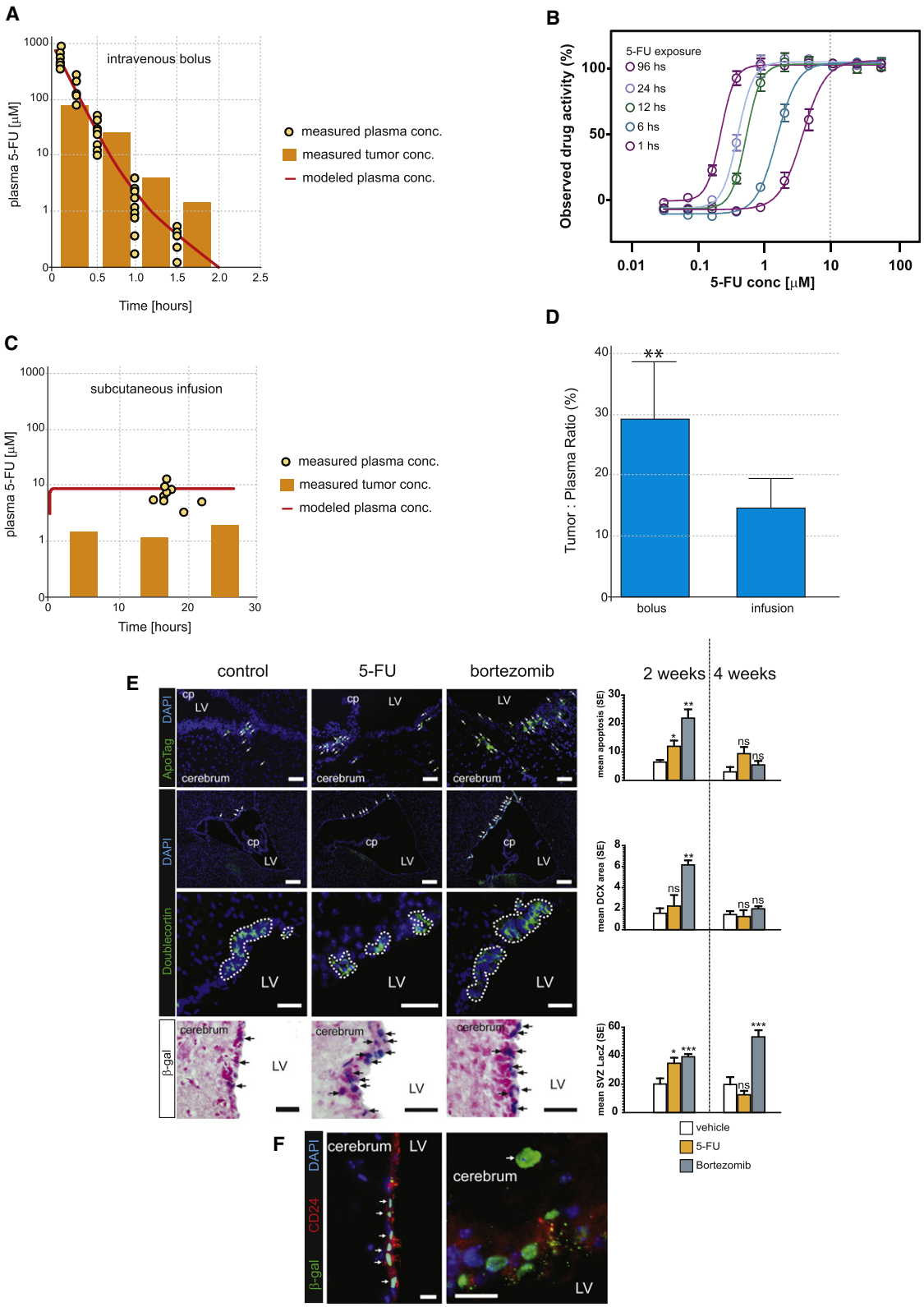

Figure 7. Pharmacokinetics and In Vivo Toxicity of 5-FU

(A) Concurrent measures of intratumoral and plasma 5-FU concentrations in ten mice that each received a single intravenous injection of 75 mg/kg of drug. (B) In vitro washout studies of 5-FU activity against mEP^{Ephb2} cells. Cells were incubated for the indicated time period with 5-FU and then to a total of 96 hr without drug. Dotted line denotes the concentration maintained in mEP^{Ephb2} tumors in the brain for at least 1 hr following bolus administration.

of a compound to compete with an immobilized, active-site directed ligand. The assay is performed by combining three components: DNA-tagged kinase; immobilized ligand; and a test compound. The ability of the test compound to compete with the immobilized ligand is measured via quantitative PCR of the DNA tag.

Ependymoma Allografts

Cells (1.5×10^6 $mEP^{Ephb2\text{-}LUC}$) resuspended in 5 μl of Matrigel (BD BioScience) were implanted into the cerebral cortex of 6- to 8-week-old CD-1 nu/nu immunocompromised mice exactly as described (Johnson et al., 2010). Mice were subject to daily clinical assessment of neurological function and weekly bioluminescence. Briefly, animals were injected with 200 μl of an aqueous solution of D-luciferin (15 mg/ml, Caliper Life Sciences) approximately 5 min prior to being imaged using an IVIS200 in vivo imaging system (Xenogen, Caliper Life Sciences). A pseudocolor image representing light intensity was generated and the relative light intensity (photons/second) from each mouse was quantified using LivingImage 4.0 software (Xenogen). For drug efficacy studies, agents were administered to mice beginning seven days post implantation when tumor luminescence ranged from $1.7–8.0 \times 10^7$ photons/sec. Mice displaying signs of excessive morbidity or toxicity (>20% weight loss) were euthanized.

Animals were treated with compounds as described in Table 1 and all drugs with the exception of lapatinib were acquired as patient preparations from the Pharmacy at St Jude Children's Research Hospital. 5-FU, topotecan and carboplatin were diluted to the required concentration in sterile water while bortezomib and irinotecan were diluted in sterile PBS. Lapatinib (LC labs) was suspended in a solution of 0.5% hydroxypropylmethylcellulose/0.1% Tween 80 and administered by gavage.

5-FU Pharmacokinetic Studies

CD-1 nude mice aged ≥8 weeks (23–28 g) were studied. Mice received a bolus tail vein injection of 5-FU (75 mg/kg) and blood samples collected at 5, 15, 30, 60, and 90 min post injection. For infusion studies, mice received an infusion of 5-FU (13 mg/kg/hr) via subcutaneous Alzet pumps (model 2001D; Cupertino, CA) and blood samples were taken at 24, 48, and 72 hr post pump implantation. 5-FU levels were determined in blood samples using a modified previously described HPLC method (Alsarra and Alarifi, 2004). Penetration of 5-FU into orthotopically implanted mEP^{Ephb2} brain tumors following intravenous bolus or subcutaneous infusion was assessed using a previously published microdialysis technique (Zhuang et al., 2006).

In Vivo Assessment of Drug Toxicity

Mice where Prom1-expressing cells are marked with LacZ (Zhu et al., 2009) were treated with 5-FU or Bortezomib either chronically (4 weeks) or acutely (two doses). The brains of these mice were fixed for frozen sectioning and processed as follows by investigators blinded to treatment group. Sagittal sections spanning the entire thickness of each brain were reviewed and three sections selected from equivalent positions in each brain representing the medial, mid and lateral aspects of the lateral ventricle. The three sections from each of the three points in the lateral ventricle were stained for LacZ, ApoTag or DCX. LacZ staining was performed and counterstained with nuclear-fast red as described (Zhu et al., 2009). Apoptosis within the SVZ was measured using the Apoptag fluorescein in situ apoptosis detection kit (Millipore). DCX immunofluorescence was performed using standard methods. Tiled images of the entire lateral ventricle were generated using a Zeiss microscope (Axio Imager M2) and processed using AxioVision Rel 4.8. Antibodies used include DCX (Santa Cruz #sc-8066), CD24 (BD #557436), and LacZ (β-galactosidase, MP Biomedicals #55976).

SUPPLEMENTAL INFORMATION

Supplemental Material includes Experimental Procedures, two figures, and one table and can be found online at doi:10.1016/j.ccr.2011.08.013.

ACKNOWLEDGMENTS

R.J.G. holds the Howard C. Schott Research Chair from the Malia's Cord Foundation. R.K.G. holds the Robert J. Ullrich Chair in Chemical Biology and Therapeutics. This work was supported by grants from the National Institutes of Health (R.J.G., R01CA129541, P01CA96832 and P30CA021765), and the Collaborative Ependymoma Research Network (R.J.G., R.K.G., C.F.S., W.K.A.Y., W.P.) and by the American Lebanese Syrian Associated Charities. We are grateful to the staff of the Hartwell Center for Bioinformatics and Biotechnology, the AIC and the ARC at St Jude Children's Research Hospital for technical assistance.

Received: January 24, 2011
Revised: June 13, 2011
Accepted: August 12, 2011
Published: September 12, 2011

REFERENCES

Adams, J. (2004). The proteasome: a suitable antineoplastic target. Nat. Rev. Cancer *4*, 349–360.

Aguirre, A., Rubio, M.E., and Gallo, V. (2010). Notch and EGFR pathway interaction regulates neural stem cell number and self-renewal. Nature *467*, 323–327.

Alsarra, I.A., and Alarifi, M.N. (2004). Validated liquid chromatographic determination of 5-fluorouracil in human plasma. J. Chromatogr. B Analyt. Technol. Biomed. Life Sci. *804*, 435–439.

Baker, K.L., Daniels, S.B., Lennington, J.B., Lardaro, T., Czap, A., Notti, R.Q., Cooper, O., Isacson, O., Frasca, S., Jr., and Conover, J.C. (2006). Neuroblast protuberances in the subventricular zone of the regenerative MRL/MpJ mouse. J. Comp. Neurol. *498*, 747–761.

Berry, D.A., Cronin, K.A., Plevritis, S.K., Fryback, D.G., Clarke, L., Zelen, M., Mandelblatt, J.S., Yakovlev, A.Y., Habbema, J.D., and Feuer, E.J.; Cancer Intervention and Surveillance Modeling Network (CISNET) Collaborators. (2005). Effect of screening and adjuvant therapy on mortality from breast cancer. N. Engl. J. Med. *353*, 1784–1792.

Bomgaars, L., Kerr, J., Berg, S., Kuttesch, J., Klenke, R., and Blaney, S.M. (2006). A phase I study of irinotecan administered on a weekly schedule in pediatric patients. Pediatr. Blood Cancer *46*, 50–55.

Bouffet, E., and Foreman, N. (1999). Chemotherapy for intracranial ependymomas. Childs Nerv. Syst. *15*, 563–570.

Brown, J.P., Couillard-Després, S., Cooper-Kuhn, C.M., Winkler, J., Aigner, L., and Kuhn, H.G. (2003). Transient expression of doublecortin during adult neurogenesis. J. Comp. Neurol. *467*, 1–10.

Carlén, M., Meletis, K., Göritz, C., Darsalia, V., Evergren, E., Tanigaki, K., Amendola, M., Barnabé-Heider, F., Yeung, M.S.Y., Naldini, L., et al. (2009).

(C) Concurrent measures of intratumoral and plasma 5-FU concentrations in ten mice that received 13 mg/kg/hr of 5-FU via Alzet pumps.
(D) Percentage tumor:plasma AUC ratio of 5-FU delivered by 75 mg/kg bolus injection and 13 mg/kg/hr infusion (**$p < 0.005$).
(E) Left: Top panel shows ApoTag stained apoptotic cells in the lateral SVZ of $Prom1^{+/C\text{-}L}$ mice following 2 weeks of vehicle control, 5-FU (75mg/kg bolus injection) or bortezomib treatment. Middle panels show low and high power images respectively of DCX^+ neuroblast rests in the SVZ of the same mice. Bottom panel shows LacZ staining of the corresponding mice. Arrows indicate cells positive for the corresponding stain, dotted lines enclose DCX^+ areas. Scale bar = 50 μm, cp = choroid plexus, LV = lateral ventricle. Right: Graphs to the right report the patterns of for the corresponding stain in all three mice at each time point (*$p < 0.05$; ***$p < 0.0005$ relative to vehicle controls).
(F) Coimmunofluorescence of nuclear β-galactosidase expressed from the modified $Prom1^{+/C\text{-}L}$ locus and CD24. Left panel shows $Prom1^+/CD24^+$ ciliated ependymal cells. Panel to the right shows a $Prom1^+/CD24$ cell (arrow) within the SVZ. Scale bar = 20 μm.

Forebrain ependymal cells are Notch-dependent and generate neuroblasts and astrocytes after stroke. Nat. Neurosci. *12*, 259–267.

Coskun, V., Wu, H., Blanchi, B., Tsao, S., Kim, K., Zhao, J., Biancotti, J.C., Hutnick, L., Krueger, R.C., Jr., Fan, G., et al. (2008). CD133+ neural stem cells in the ependyma of mammalian postnatal forebrain. Proc. Natl. Acad. Sci. USA *105*, 1026–1031.

Cowan, C.R., and Hyman, A.A. (2006). Cyclin E-Cdk2 temporally regulates centrosome assembly and establishment of polarity in Caenorhabditis elegans embryos. Nat. Cell Biol. *8*, 1441–1447.

Dietrich, J., Han, R., Yang, Y., Mayer-Pröschel, M., and Noble, M. (2006). CNS progenitor cells and oligodendrocytes are targets of chemotherapeutic agents in vitro and in vivo. J. Biol. *5*, 22.

Douillard, J.Y., Cunningham, D., Roth, A.D., Navarro, M., James, R.D., Karasek, P., Jandik, P., Iveson, T., Carmichael, J., Alakl, M., et al. (2000). Irinotecan combined with fluorouracil compared with fluorouracil alone as first-line treatment for metastatic colorectal cancer: a multicentre randomised trial. Lancet *355*, 1041–1047.

Geoerger, B., Gaspar, N., Opolon, P., Morizet, J., Devanz, P., Lecluse, Y., Valent, A., Lacroix, L., Grill, J., and Vassal, G. (2008). EGFR tyrosine kinase inhibition radiosensitizes and induces apoptosis in malignant glioma and childhood ependymoma xenografts. Int. J. Cancer *123*, 209–216.

Gilbert, M.R., Ruda, R., and Soffietti, R. (2010). Ependymomas in adults. Curr. Neurol. Neurosci. Rep. *10*, 240–247.

Gilbertson, R.J., Bentley, L., Hernan, R., Junttila, T.T., Frank, A.J., Haapasalo, H., Connelly, M., Wetmore, C., Curran, T., Elenius, K., and Ellison, D.W. (2002). ERBB receptor signaling promotes ependymoma cell proliferation and represents a potential novel therapeutic target for this disease. Clin. Cancer Res. *8*, 3054–3064.

Gorlick, R., Kolb, E.A., Houghton, P.J., Morton, C.L., Phelps, D., Schaiquevich, P., Stewart, C., Keir, S.T., Lock, R., Carol, H., et al. (2009). Initial testing (stage 1) of lapatinib by the pediatric preclinical testing program. Pediatr. Blood Cancer *53*, 594–598.

Grunda, J.M., Fiveash, J., Palmer, C.A., Cantor, A., Fathallah-Shaykh, H.M., Nabors, L.B., and Johnson, M.R. (2010). Rationally designed pharmacogenomic treatment using concurrent capecitabine and radiotherapy for glioblastoma; gene expression profiles associated with outcome. Clin. Cancer Res. *16*, 2890–2898.

Gupta, P.B., Onder, T.T., Jiang, G., Tao, K., Kuperwasser, C., Weinberg, R.A., and Lander, E.S. (2009). Identification of selective inhibitors of cancer stem cells by high-throughput screening. Cell *138*, 645–659.

Houghton, J.A., Cheshire, P.J., Hallman, J.D., 2nd, Lutz, L., Luo, X., Li, Y., and Houghton, P.J. (1996). Evaluation of irinotecan in combination with 5-fluorouracil or etoposide in xenograft models of colon adenocarcinoma and rhabdomyosarcoma. Clin. Cancer Res. *2*, 107–118.

IMPACT. (1995). Efficacy of adjuvant fluorouracil and folinic acid in colon cancer. International Multicentre Pooled Analysis of Colon Cancer Trials (IMPACT) investigators. Lancet *345*, 939–944.

Jin, K., Wang, X., Xie, L., Mao, X.O., and Greenberg, D.A. (2010). Transgenic ablation of doublecortin-expressing cells suppresses adult neurogenesis and worsens stroke outcome in mice. Proc. Natl. Acad. Sci. USA *107*, 7993–7998.

Johnson, R.A., Wright, K.D., Poppleton, H., Mohankumar, K.M., Finkelstein, D., Pounds, S.B., Rand, V., Leary, S.E., White, E., Eden, C., et al. (2010). Cross-species genomics matches driver mutations and cell compartments to model ependymoma. Nature *466*, 632–636.

Kadota, R.P., Stewart, C.F., Horn, M., Kuttesch, J.F., Jr., Burger, P.C., Kepner, J.L., Kun, L.E., Friedman, H.S., and Heideman, R.L. (1999). Topotecan for the treatment of recurrent or progressive central nervous system tumors: a pediatric oncology group phase II study. J. Neurooncol. *43*, 43–47.

Kamano, T., Mikami, Y., and Shirasaka, T. (1997). Continuous infusion of 5-fluorouracil plus low-dose cisplatin in tumor-bearing mice. Anticancer Drugs *8*, 632–636.

Kasbek, C., Yang, C.H., Yusof, A.M., Chapman, H.M., Winey, M., and Fisk, H.A. (2007). Preventing the degradation of mps1 at centrosomes is sufficient to cause centrosome reduplication in human cells. Mol. Biol. Cell *18*, 4457–4469.

Kimura, H., Ng, J.M., and Curran, T. (2008). Transient inhibition of the Hedgehog pathway in young mice causes permanent defects in bone structure. Cancer Cell *13*, 249–260.

Kleihues, P., Louis, D.N., Scheithauer, B.W., Rorke, L.B., Reifenberger, G., Burger, P.C., and Cavenee, W.K. (2002). The WHO classification of tumors of the nervous system. J. Neuropathol. Exp. Neurol. *61*, 215–225, discussion, 226–219.

Kriegstein, A., and Alvarez-Buylla, A. (2009). The glial nature of embryonic and adult neural stem cells. Annu. Rev. Neurosci. *32*, 149–184.

Lapidot, T., Sirard, C., Vormoor, J., Murdoch, B., Hoang, T., Caceres-Cortes, J., Minden, M., Paterson, B., Caligiuri, M.A., and Dick, J.E. (1994). A cell initiating human acute myeloid leukaemia after transplantation into SCID mice. Nature *367*, 645–648.

Lehtinen, M.K., Zappaterra, M.W., Chen, X., Yang, Y.J., Hill, A.D., Lun, M., Maynard, T., Gonzalez, D., Kim, S., Ye, P., et al. (2011). The cerebrospinal fluid provides a proliferative niche for neural progenitor cells. Neuron *69*, 893–905.

Lens, S.M., Voest, E.E., and Medema, R.H. (2010). Shared and separate functions of polo-like kinases and aurora kinases in cancer. Nat. Rev. Cancer *10*, 825–841.

Lesage, B., Gutierrez, I., Marti, E., and Gonzalez, C. (2010). Neural stem cells: the need for a proper orientation. Curr. Opin. Genet. Dev. *20*, 438–442.

Longley, D.B., Harkin, D.P., and Johnston, P.G. (2003). 5-Fluorouracil: mechanisms of action and clinical strategies. Nat. Rev. Cancer *3*, 330–338.

McGuire, C.S., Sainani, K.L., and Fisher, P.G. (2009). Incidence patterns for ependymoma: a surveillance, epidemiology, and end results study. J. Neurosurg. *110*, 725–729.

Mendrzyk, F., Korshunov, A., Benner, A., Toedt, G., Pfister, S., Radlwimmer, B., and Lichter, P. (2006). Identification of gains on 1q and epidermal growth factor receptor overexpression as independent prognostic markers in intracranial ependymoma. Clin. Cancer Res. *12*, 2070–2079.

Merchant, T.E., Li, C., Xiong, X., Kun, L.E., Boop, F.A., and Sanford, R.A. (2009). Conformal radiotherapy after surgery for paediatric ependymoma: a prospective study. Lancet Oncol. *10*, 258–266.

Neal, J.W., and Sequist, L.V. (2010). Exciting new targets in lung cancer therapy: ALK, IGF-1R, HDAC, and Hh. Curr. Treat. Options Oncol. *11*, 36–44.

Noatynska, A., Panbianco, C., and Gotta, M. (2010). SPAT-1/Bora acts with Polo-like kinase 1 to regulate PAR polarity and cell cycle progression. Development *137*, 3315–3325.

Phuphanich, S., Supko, J.G., Carson, K.A., Grossman, S.A., Burt Nabors, L., Mikkelsen, T., Lesser, G., Rosenfeld, S., Desideri, S., and Olson, J.J. (2010). Phase 1 clinical trial of bortezomib in adults with recurrent malignant glioma. J. Neurooncol. *100*, 95–103.

Pui, C.-H., Relling, M.V., and Downing, J.R. (2004). Acute lymphoblastic leukemia. N. Engl. J. Med. *350*, 1535–1548.

Richardson, P.G., Barlogie, B., Berenson, J., Singhal, S., Jagannath, S., Irwin, D., Rajkumar, S.V., Srkalovic, G., Alsina, M., Alexanian, R., et al. (2003). A phase 2 study of bortezomib in relapsed, refractory myeloma. N. Engl. J. Med. *348*, 2609–2617.

Romer, J.T., Kimura, H., Magdaleno, S., Sasai, K., Fuller, C., Baines, H., Connelly, M., Stewart, C.F., Gould, S., Rubin, L.L., and Curran, T. (2004). Suppression of the Shh pathway using a small molecule inhibitor eliminates medulloblastoma in Ptc1(+/-)p53(-/-) mice. Cancer Cell *6*, 229–240.

Rudin, C.M., Hann, C.L., Laterra, J., Yauch, R.L., Callahan, C.A., Fu, L., Holcomb, T., Stinson, J., Gould, S.E., Coleman, B., et al. (2009). Treatment of medulloblastoma with hedgehog pathway inhibitor GDC-0449. N. Engl. J. Med. *361*, 1173–1178.

Singh, S.K., Hawkins, C., Clarke, I.D., Squire, J.A., Bayani, J., Hide, T., Henkelman, R.M., Cusimano, M.D., and Dirks, P.B. (2004). Identification of human brain tumour initiating cells. Nature *432*, 396–401.

Stewart, C.F., Iacono, L.C., Chintagumpala, M., Kellie, S.J., Ashley, D., Zamboni, W.C., Kirstein, M.N., Fouladi, M., Seele, L.G., Wallace, D., et al.

(2004). Results of a phase II upfront window of pharmacokinetically guided topotecan in high-risk medulloblastoma and supratentorial primitive neuroectodermal tumor. J. Clin. Oncol. *22*, 3357–3365.

Taniguchi, E., Cho, M.J., Arenkiel, B.R., Hansen, M.S., Rivera, O.J., McCleish, A.T., Qualman, S.J., Guttridge, D.C., Scott, M.P., Capecchi, M.R., and Keller, C. (2009). Bortezomib reverses a post-translational mechanism of tumorigenesis for patched1 haploinsufficiency in medulloblastoma. Pediatr. Blood Cancer *53*, 136–144.

Taylor, M.D., Poppleton, H., Fuller, C., Su, X., Liu, Y., Jensen, P., Magdaleno, S., Dalton, J., Calabrese, C., Board, J., et al. (2005). Radial glia cells are candidate stem cells of ependymoma. Cancer Cell *8*, 323–335.

Thompson, J., Zamboni, W.C., Cheshire, P.J., Lutz, L., Luo, X., Li, Y., Houghton, J.A., Stewart, C.F., and Houghton, P.J. (1997). Efficacy of systemic administration of irinotecan against neuroblastoma xenografts. Clin. Cancer Res. *3*, 423–431.

Tonda, M.E., Heideman, R.L., Petros, W.P., Friedman, H.S., Murry, D.J., and Rodman, J.H. (1996). Carboplatin pharmacokinetics in young children with brain tumors. Cancer Chemother. Pharmacol. *38*, 395–400.

Wagner, L.M., Perentesis, J.P., Reid, J.M., Ames, M.M., Safgren, S.L., Nelson, M.D., Jr., Ingle, A.M., Blaney, S.M., and Adamson, P.C. (2010). Phase I trial of two schedules of vincristine, oral irinotecan, and temozolomide (VOIT) for children with relapsed or refractory solid tumors: a Children's Oncology Group phase I consortium study. Pediatr. Blood Cancer *54*, 538–545.

Wang, Y., Lian, L., Golden, J.A., Morrisey, E.E., and Abrams, C.S. (2007). PIP5KI gamma is required for cardiovascular and neuronal development. Proc. Natl. Acad. Sci. USA *104*, 11748–11753.

Wang, X., Tsai, J.W., Imai, J.H., Lian, W.N., Vallee, R.B., and Shi, S.H. (2009). Asymmetric centrosome inheritance maintains neural progenitors in the neocortex. Nature *461*, 947–955.

Williamson, M.J., Silva, M.D., Terkelsen, J., Robertson, R., Yu, L., Xia, C., Hatsis, P., Bannerman, B., Babcock, T., Cao, Y., and Kupperman, E. (2009). The relationship among tumor architecture, pharmacokinetics, pharmacodynamics, and efficacy of bortezomib in mouse xenograft models. Mol. Cancer Ther. *8*, 3234–3243.

Yu, Y.-L., Chou, R.-H., Chen, L.-T., Shyu, W.-C., Hsieh, S.-C., Wu, C.-S., Zeng, H.-J., Yeh, S.-P., Yang, D.-M., Hung, S.-C., and Hung, M.-C. (2011). EZH2 regulates neuronal differentiation of mesenchymal stem cells through PIP5K1C-dependent calcium signaling. J. Biol. Chem. *286*, 9657–9667.

Zhou, B.-B.S., Zhang, H., Damelin, M., Geles, K.G., Grindley, J.C., and Dirks, P.B. (2009). Tumour-initiating cells: challenges and opportunities for anticancer drug discovery. Nat. Rev. Drug Discov. *8*, 806–823.

Zhu, L., Gibson, P., Currle, D.S., Tong, Y., Richardson, R.J., Bayazitov, I.T., Poppleton, H., Zakharenko, S., Ellison, D.W., and Gilbertson, R.J. (2009). Prominin 1 marks intestinal stem cells that are susceptible to neoplastic transformation. Nature *457*, 603–607.

Zhuang, Y., Fraga, C.H., Hubbard, K.E., Hagedorn, N., Panetta, J.C., Waters, C.M., and Stewart, C.F. (2006). Topotecan central nervous system penetration is altered by a tyrosine kinase inhibitor. Cancer Res. *66*, 11305–11313.